Title

Analysis of Screening Current Effects in a Hybrid Nb$_{3}$Sn/REBCO Superconducting Accelerator Magnet Using a T-A Formulation

Journal

IEEE Transactions on Applied Superconductivity, 35(5)

ISSN

1051-8223

Authors

Yang, Ye
Yan, Yufan
Kurian, Febin
et al.

Publication Date

2025-08-01

DOI

10.1109/tasc.2025.3528378

Analysis of Screening Current Effects in a Hybrid Nb_3Sn/REBCO Superconducting Accelerator Magnet Using a *T*-*A* Formulation

Ye Yang, Yufan Yan, Febin Kurian, Mukesh Dhakarwal, Masami Iio, Kento Suzuki, Xiaorong Wang, Ramesh Gupta, Toru Ogitsu, and Tengming Shen *Senior Member, IEEE*

***Abstract*—To explore the feasibility of using high-temperature superconducting (HTS) REBCO coated conductors in future accelerator magnets, two REBCO flat racetrack coils were fabricated using 4-mm wide EuBCO tapes at the High Energy Accelerator Research Organization (KEK). These coils were tested as an insert inside a Nb_3Sn common-coil dipole magnet, which provides a background field of up to ∼9.5 T, at the Brookhaven National Laboratory (BNL). REBCO tapes offer exceptionally high critical current density under strong magnetic fields; however, they also exhibit significant magnetization due to screening currents, leading to magnetic field errors. This study presents a 2D finite element model of screening current-induced fields (SCIF) in REBCO coils using the *T-A* formulation, along with the results obtained. Simulations were then performed for two KEK test cases: one where the REBCO conductors were oriented with the HTS tapes parallel to the background field, and another where the tapes were perpendicular to it. Since screening currents also influence the stress distribution and increase the peak stress in the coils, the mechanical effects of these currents were analyzed. The implications of these simulation and test results for the design of Nb_3Sn/REBCO superconducting accelerator magnets are discussed.**

***Index Terms*—Accelerator magnets, Common-coil dipole, HTS insert coil, Hybrid magnet, Screening current**

I. Introduction

HIGH-temperature superconducting (HTS) cuprate conductors, including both BSCCO and REBCO, have been developed into practical metal/superconductor composite conductors and are commercially available in lengths suitable for magnet applications [1], [2], such as nuclear magnetic resonance [3], fusion [4], and high-energy physics facilities. Some HTS devices will enable new high-energy physics facilities and experiments with unprecedented capabilities [5], [6]. Examples include a high-energy upgrade of the LHC using 20 T accelerator magnets, which have 2.5 times the field strength of existing LHC Nb-Ti magnets and exceed the capabilities of Nb-Ti and Nb_3Sn magnet technologies, achieving a maximal center-of-mass collision energy of 33 TeV, and a multi-TeV muon collider [7]. In addition, some devices will enable significant improvements in power efficiency, especially within high-radiation environments, by replacing resistive magnets or by raising the opeartion temperature of superconducting magnets from 4.2 K (liquid helium cooled) to 20-50 K (conductively cooled by cryocoolers). Examples include focusing solenoid magnets for positron sources for lepton accelerators [8] and solenoids to capture secondary particles, such as pions, produced at targets in high-intensity accelerator facilities [9].

There have been extensive studies and significant advances in key technologies of REBCO solenoids, such as insulation, field quality control, and stress management in recent years; For the accelerator magnets, the REBCO coil is usually employed as an insert in a Nb_3Sn/REBCO hybrid dipole magnet. For developing high-field hybrid magnets, orienting the HTS coil parallel to the background field offers significant advantages, including the ability to achieve higher magnetic fields and reduced field changes. This design philosophy has been a milestone in the development of FEATHER magnets, an aligned-block REBCO dipole magnet [10], [11].

The purpose of this work is to investigate the potential of using high-temperature superconducting REBCO-coated conductors to construct future accelerator magnets. Two racetrack coils were fabricated at the High Energy Accelerator Research Organization (KEK) using 4-mm wide EuBCO tapes insulated with radiation-resistant ceramic insulation material [12]. The coils were then tested at the Brookhaven National Laboratory (BNL) as inserts inside a Nb_3Sn common-coil dipole magnet, which can provide a background field of up to ∼9.5 T. An important technical issue revealed in solenoid studies is the critical role of screening currents in determining the operational limits and post-quench survival of REBCO coils in high magnetic fields [13]–[15]. In this study, we analyze two test cases with a 2D finite element model based on the *T-A* formulation [16]. We then evaluate screening current distributions and coil stresses considering screening current effects in two cases that the HTS insert coil is parallel and perpendicular to the background field.

The work at was supported by the U.S. Department of Energy (DOE), Office of Science under contract no. DE-AC02-05CH11231.

Y. Yang, Y. Yan, X. Wang and T. Shen are with Lawrence Berkeley National Laboratory (LBNL), 1 Cyclotron Road, Berkeley, CA 94720, USA (e-mail: yeyang@lbl.gov).

M. Dhakarwal, M. Iio, K. Suzuki and T. Ogitsu are with High Energy Accelerator Research Organization (KEK), 1-1 Oho, Tsukuba, Ibaraki, 305-0801, Japan.

F. Kurian and R. Gupta are with Brookhaven National Laboratory (BNL), Upton, NY 11973, USA.

II. Model description

A. Coil configuration

Fig. 1 shows the schematics of the magnetic and mechanical models. The Nb_3Sn common-coil dipole magnet DCC017 at

This article has been accepted for publication in IEEE Transactions on Applied Superconductivity. This is the author's version which has not been fully edited and content may change prior to final publication. Citation information: DOI 10.1109/TASC.2025.3528378

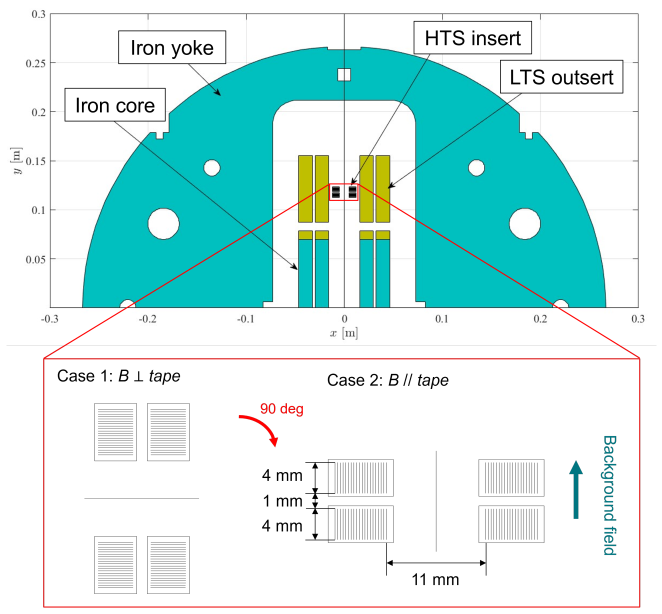

Fig. 1. Magnetic model for simulating screening current effects. The upper one presents the global geometry of the HTS / LTS hybrid magnet, where two racetrack coils are placed in the background field perpendicular (case 1) and parallel (case 2) to the HTS tape. The lower one shows the details of the HTS coil aligned in the field of the LTS magnet.

TABLE I
PARAMETERS OF THE HTS INSERT IN THE HYBRID SETUP

Item	Unit	Value
HTS tape width	mm	4.0
HTS tape thickness	mm	0.16
Thickness of HTS film	μm	2.5
Insulation thickness on each side	mm	0.10
Total number of turns	-	20
n-value	-	45

BNL can provide a background dipole field of up to ∼9.5 T with a nominal current of 10 kA [17]. It features a large aperture of 31×338 mm^2 to accommodate two HTS insert coils.

The HTS insert coil consists of two racetrack coils, each wound with 20 turns around the pole, with a minimum bending radius of 5.5 mm and a distance of 11 mm between the innermost layers. To investigate the screening current effects based on conductor orientation, the HTS coil was positioned in one of the common-coil apertures in the following configurations:

1) Background field perpendicular to the HTS tape.
2) Background field parallel to the HTS tape.

The HTS insert does not include a bore; instead, a Hall sensor is embedded at the center of the pole for field measurements. The coil parameters are listed in Table I. The HTS insert and LTS outsert are charged with the independent power supplies. The HTS inserts in configurations 1) and 2) generate the main dipole fields in the horizontal and vertical directions, respectively.

B. Magnetic and mechanical models

The screening current is analyzed in this study using the $T-A$ formulation [16]. The governing equations are given

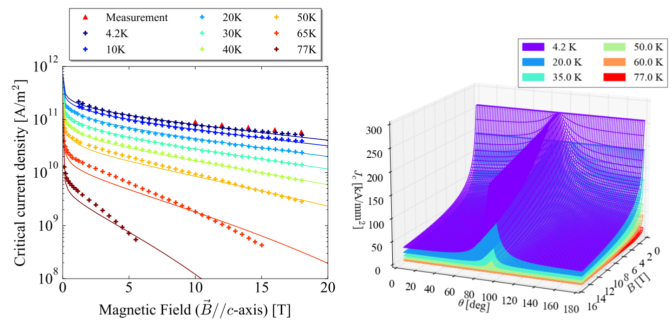

Fig. 2. Critical current density as a function of temperature, magnetic field, and angle used in the simulation. Data shown in cross symbols was provided by Fujikura Ltd. [18], and data with triangle symbols were measured by KEK [12]. The lines represent fitted curves used in the models.

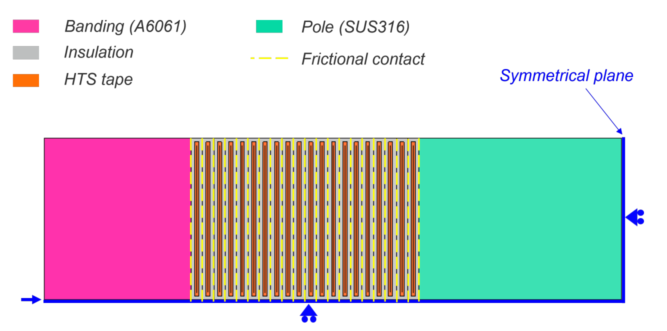

Fig. 3. Mechanical model for simulating the stress with the imported screening current distribution. The roller constraints are applied to the symmetrical planes, and the limited horizontal displacement with the range from -inf. to 0 is added to the edge of the aluminum banding to improve the calculation convergence. The contact between each layer is frictional to each other.

by

$$\nabla \times (\rho_{HTS} \nabla \times T\vec{n}) \cdot \vec{n} + \frac{\partial(\vec{B}\cdot\vec{n})}{\partial t} = 0 \quad (1)$$

$$\nabla \times (\nu \nabla \times \vec{A}) - \vec{J} = 0 \quad (2)$$

where T is the magnitude of the current vector potential, $\vec{n}$ is the unit normal vector at the current source point perpendicular to the HTS tape surface, $\vec{J}$ is the current density vector, ν is the reluctivity, which is related to the nonlinear $B-H$ curve of the iron yoke, and $\vec{A}$ is the magnetic vector potential. The T formulation is applied in the superconductor region, while the A formulation is applied in all regions. The resistivity of the HTS film is expressed as

$$\rho_{HTS} = \frac{E_c}{J_c(T,B,\theta)} \left| \frac{\vec{J}}{J_c(T,B,\theta)} \right|^{n-1} \quad (3)$$

where $E_c = 0.1$ μV/cm is the critical electric field, and J_c is the critical current density as a function of temperature, magnetic field, and angle. A current constraint is applied as a boundary condition at the edges of the HTS film, given by

$$I_t = \int \vec{J} dA = \oint \vec{T} dl = (T_1 - T_2)\delta \quad (4)$$

where I_t is the transport current, δ is the HTS film thickness, and T_1, T_2 are the current vector potentials at the two edges of the HTS tape.

This article has been accepted for publication in IEEE Transactions on Applied Superconductivity. This is the author's version which has not been fully edited and content may change prior to final publication. Citation information: DOI 10.1109/TASC.2025.3528378

TABLE II
MATERIAL PROPERTIES FOR THE HTS TAPE BEFORE INSULATION

Item	Unit	Value					
Material	-	Cu	Hastelloy	Ag	EuBCO	Buffer	Total
Thickness	μm	80	75	2	2.5	0.7	160.2
Young's modulus	GPa	40	210	90	180	90	122.6

Fig. 2 shows the critical current density (J_c) curves used in the simulation. We adopted the model proposed in [19] to fit the critical current measurements conducted by KEK [12] and the data provided by Fujikura Ltd. [18]. The measurements were performed under external fields ranging from 10 T to 15 T applied along the c-axis of the tape at 4.2 K. In this model, the angular dependency was preserved as originally proposed, while the J_c field and temperature dependencies were fitted using the data for fields perpendicular and parallel to the tape.

A separate mechanical model was developed to further evaluate screening current-induced mechanical stresses in one quadrant of the HTS insert coil, as shown in Fig. 3. The Young's modulus of the non-insulated HTS tape was aver-aged using the material properties of REBCO, Hastelloy, and copper, as listed in Table II, following the approach described in [20]. The thermal expansion coefficient of the HTS tape was assumed to be $11 \times 10^{-6}\,\mathrm{K}^{-1}$. In this study, the non-insulated HTS tapes were coated with a ceramic spray, and the coil was wound wet using a ceramic adhesive. Due to the expected weak bonding between turns, the model assumes that each ceramic insulated tape is in contact with neighboring turns with a friction coefficient of 0.2. The contacts between the pole and the HTS coil, as well as between the banding and the HTS coil, were also modeled as frictional contacts.

The simulation includes two steps: cool-down to 4.2 K and energization. A preload is applied to the HTS coil to counteract the total magnetic force by introducing an opposing force through a 4-mm thick aluminum banding. The final preload state is achieved after the cool-down process. In this study, we did not consider the specific method for applying the preload to the HTS insert coil. Potentially, the "bladder & key" technology, combined with banding tension, could be utilized in a practical implementation.

III. CASE STUDIES

Fig. 4 shows the simulation results for ramping the hybrid magnet in the two orientations. To evaluate the influence of screening currents, the Nb_3Sn magnet was first charged to its nominal current of 10 kA, followed by the energization of the HTS insert coil through two cycles, reaching up to approximately 70% of J_c. Due to the angular dependence of J_c, the HTS insert coil can operate at currents up to 1 kA in the parallel case, which is roughly double the maximum current achieved in the perpendicular case.

A. Screening current induced magnetic field

The multipole field harmonics and the field changes within the range between the injection and extraction fields are critical for accelerator magnets [21]. Since this HTS insert is not designed to minimize field errors, we do not discuss harmonics in this study and instead focus on the variation of the central field. Fig. 5 shows the changes in the magnetic field at the center of the HTS insert coils. For the perpendicular case, as shown in Fig. 6, the screening current fully penetrates the HTS tape, and most of the screening current-induced field (SCIF) is generated during the energization of the outsert. The maximum field change is approximately -250 mT at the start of the ramp, decreasing to around -150 mT in the high-current region due to the reduction in J_c. During the discharge of the Nb_3Sn magnet, the field change increases again, reaching up to 300 mT at zero current.

In contrast, when the outsert field is parallel to the HTS tape, the screening current penetrates the HTS tape more gradually even at high magnetic fields, due to the weak horizontal component of the external field. At the nominal current of the LTS outsert, the screening current is primarily concentrated at the edges of the HTS tape. Consequently, the central field changes by less than 10 mT, which is significantly lower than in the perpendicular case. After the HTS insert coil is energized, it generates a horizontal field, enabling further penetration of the screening current into the HTS tape. This leads to an 80-mT field change at the hybrid magnet's nominal current, as shown in Fig. 5.

These results indicate that the perpendicular case introduces a substantial field error at the magnet center, which is undesirable for accelerator magnets. In other words, adjusting the orientation of the HTS tape can effectively reduce the field error.

B. Screening current induced stress

The mechanical behavior of the HTS insert coils is also influenced by screening currents. Fig. 7 illustrates the magnetic force distributions at the hybrid magnet's nominal current, with and without considering the screening current effect. In the perpendicular case, the force density with the screening current effect is similar to that without it. The force direction is entirely parallel to the tape surface, subjecting the tapes to compressive forces. In contrast, in the parallel case, most forces are perpendicular to the tapes, and the force density distributions differ significantly depending on whether the screening current effect is considered. As described in the previous section, the screening current does not fully penetrate the HTS tapes and the higher J_c, resulting in huge forces that primarily concentrate at the edges of the tapes. This may result in bending stress concentrated close to the tape edges, potentially causing greater degradation of the HTS insert coil compared to the perpendicular case.

A mechanical analysis was also conducted to investigate the effects of screening current-induced stress using the calculated force density. Similar to general superconducting accelerator magnets, preload is applied to prevent overstress in the HTS tape. Fig. 8 illustrates the horizontal stress distribution in the HTS insert coil, with and without the consideration of the screening current effect. Due to the preload, the HTS insert coil remains under compression after energization. In the parallel case, excluding the localized stress concentration

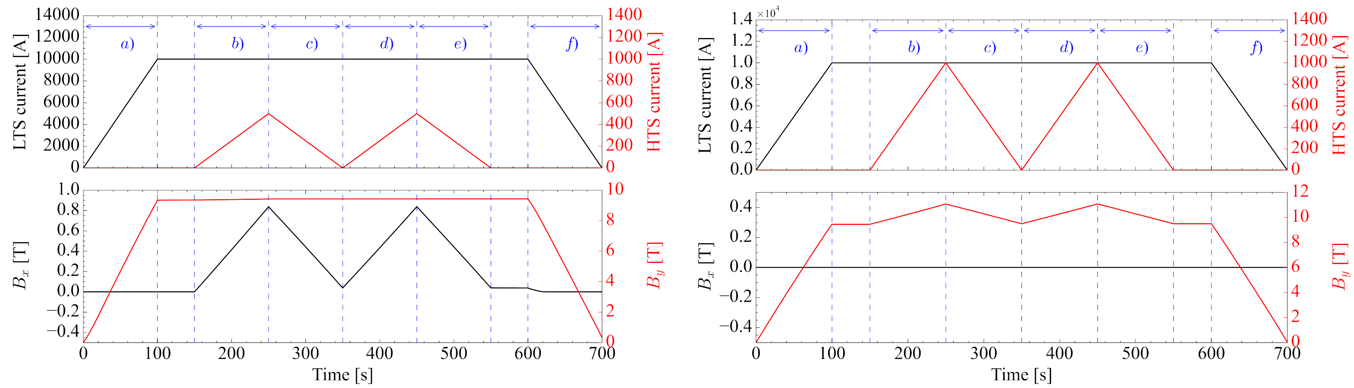

(a) $\vec{B} \perp$ HTS tape

(b) $\vec{B}$ // HTS tape

Fig. 4. Ramping the hybrid magnet up to about 70% of J_c(4.2 K, B_{op}, θ))for the HTS insert coils. The red and black lines in the upper figures indicate the currents in the Nb_3Sn and HTS coils, respectively. The red and black lines in the lower figures show the x and y components of the magnetic field generated by the hybrid magnet.

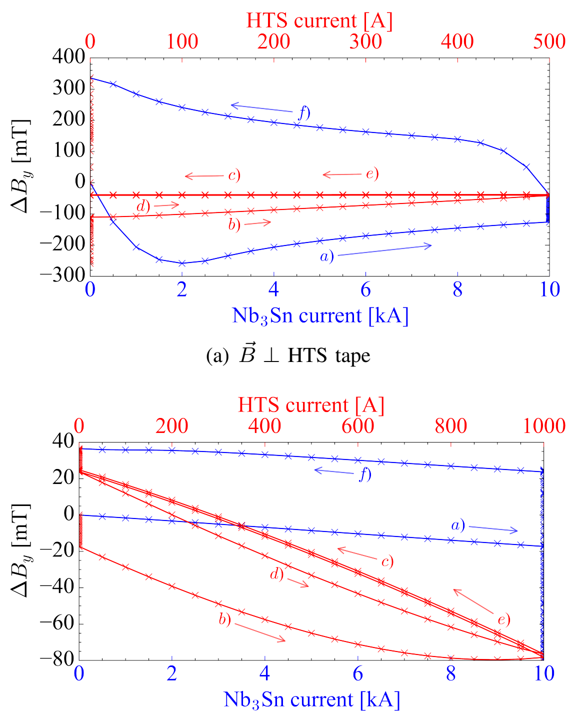

(a) $\vec{B} \perp$ HTS tape

(b) $\vec{B}$ // HTS tape

Fig. 5. The change in the magnetic field at the center of the HTS coils for two cases. The red and blue lines represent the field change, accounting for the screening current effect contributed by the HTS insert and Nb_3Sn magnet ramping.

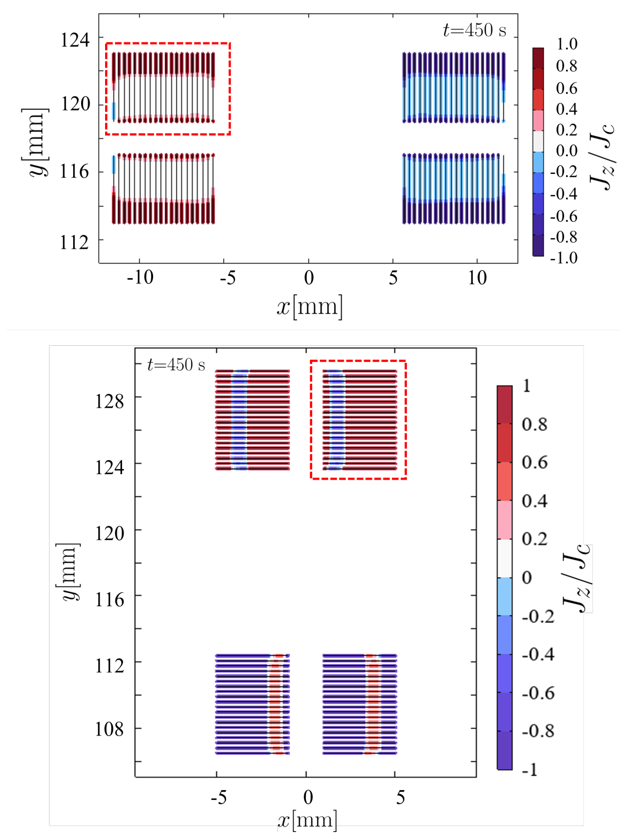

Fig. 6. Screening current distribution in the HTS insert at 450 s when both the HTS insert and the LTS outsert reach the nominal currents. The upper and lower figures show the fields parallel and perpendicular to the HTS tapes, respectively. The red dot line indicate the HTS insert quadrant for the mechanical analysis.

at the tape edges, the maximum stress after cool-down is -77 MPa, which increases to -70 MPa when the hybrid magnet is energized to its nominal current. With the preload, the stress distribution closely resembles that observed without the screening current effect. This indicates that the preload process plays a critical role in mitigating the complex magnetic forces induced by the screening current.

In the perpendicular case, since the horizontal component of the magnetic force dominates (see Fig. 7), the vertical preload does not directly cancel the magnetic force. The maximum stress is -28 MPa after cool-down, and it decreases to -66 MPa after energization. As the screening current effect does not significantly change the force density distribution, the stress distribution in the perpendicular case is very similar to that observed without considering the screening current effect.

For REBCO-coated conductors, the critical current remains

This article has been accepted for publication in IEEE Transactions on Applied Superconductivity. This is the author's version which has not been fully edited and content may change prior to final publication. Citation information: DOI 10.1109/TASC.2025.3528378

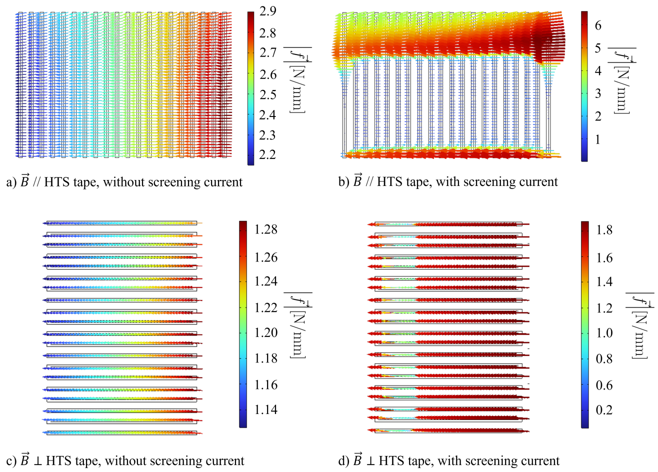

Fig. 7. Magnetic force density distribution at the hybrid magnet nominal current (450 s). The left and right two figures represent the force density without and with the consideration of the screening current effect.

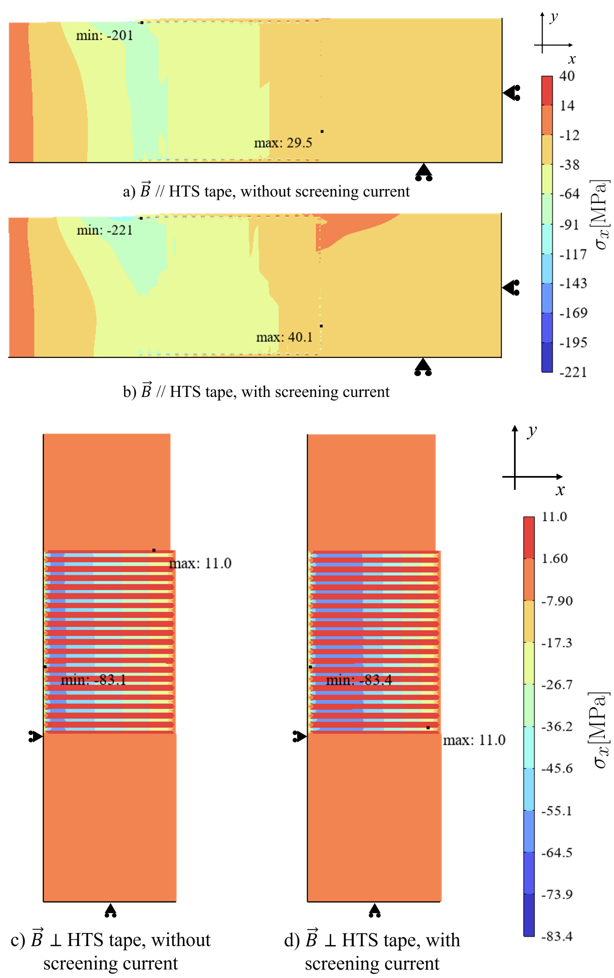

Fig. 8. Horizontal stress distribution in the HTS insert coil at the nominal current of the hybrid magnet (450 s). The top figure corresponds to the parallel case, while the bottom figure represents the perpendicular case.

nearly constant across a wide strain range from -1.2% to +0.45% [22], corresponding to stress values ranging from -1440 MPa to 540 MPa. Therefore, we do not expect any degradation of the critical current during energization.

IV. Conclusion

This paper analyzed and compared the screening current effects in an HTS racetrack insert placed in two different orientations within a Nb_3Sn common-coil magnet. Screening currents play important but very different roles in these two cases. A large field error is induced with the background field applied perpendicular to the tape but the screening current tends to have a small role in modifying magnetic force. In contrast, a smaller field is induced by screening current with the background field applied parallel to the tape but the screening current modifies the magnetic force significantly. Additionally, the magnetic force concentrates at the edge of the tape because the screening current does not fully penetrate the tape. With the preload suppressing the HTS insert coil against the magnetic force, no degradation of the critical current is expected for either orientation even considering the screening current effect.

Acknowledgment

This work was supported by the U.S. Department of Energy, Office of High Energy Physics U.S.-Japan Science and Technology Cooperation Program. The work at LBNL was also supported by the U.S. Department of Energy (DOE), Office of Science under contract no. DE-AC02-05CH11231.

References

[1] T. Shen and L. Garcia Fajardo, "Superconducting accelerator magnets based on high-temperature superconducting bi-2212 round wires," *Instruments*, vol. 4, no. 2, p. 17, 2020.

[2] H. Weijers, U. Trociewitz, W. Markiewicz, J. Jiang, D. Myers, E. Hellstrom, A. Xu, J. Jaroszynski, P. Noyes, Y. Viouchkov *et al.*, "High field magnets with HTS conductors," *IEEE Trans. Appl. Supercond.*, vol. 20, no. 3, pp. 576–582, 2010.

[3] Y. Yanagisawa, R. Piao, Y. Suetomi, T. Yamazaki, K. Yamagishi, T. Ueno, T. Takao, K. Ohki, T. Yamaguchi, T. Nagaishi, H. Kitaguchi, Y. Miyoshi, M. Yoshikawa, M. Hamada, K. Saito, K. Hachitani, Y. Ishii, and H. Maeda, "Development of a persistent-mode nmr magnet with superconducting joints between high-temperature superconductors," *Superconductor Science and Technology*, vol. 34, no. 11, p. 115006, sep 2021. [Online]. Available: https://dx.doi.org/10.1088/1361-6668/ac2120

[4] M. J. Wolf, C. Ebner, W. H. Fietz, R. Heller, D. Nickel, and K.-P. Weiss, "High temperature superconductors for fusion applications and new developments for the hts croco conductor design," *Fusion Engineering and Design*, vol. 172, p. 112739, 2021. [Online]. Available: https://www.sciencedirect.com/science/article/pii/S0920379621005159

[5] G. Vallone, D. Arbelaez, D. M. Araujo, A. Ballarino, P. Ferracin, A. Hafalia, S. Hopkins, V. Marinozzi, I. Pong, S. Prestemon, G. Sabbi, and G. Velev, "Magnetic and Mechanical Analysis of a Large Aperture 15 T Cable Test Facility Dipole Magnet," *IEEE Trans. Appl. Supercond.*, vol. 31, no. 5, 2021, Art. no. 9500406.

[6] J. L. R. Fernández, D. Arbelaez, P. Ferracin, R. Hafalia, R. Lee, P. Mallon, S. Prestemon, G. Sabbi, T. Tristan, and G. Vallone, "Engineering Design of a Large Aperture 15 T Cable Test Facility Dipole Magnet," *IEEE Trans. Appl. Supercond.*, vol. 32, no. 6, 2022, Art. no. 9500605.

[7] L. Bottura, C. Accettura, N. Amemiya, B. Auchmann, J. Berg, A. Bersani, A. Bertarelli, F. Boattini, B. Bordini, P. Borges de Sousa, M. Breschi, B. Caiffi, X. Chaud, F. Debray, A. Dudarev, M. Eisterer, S. Fabbri, S. Farinon, P. Ferracin, H. De Gersem, A. Kario, A. Kolehmainen, J. Kosse, J. Lorenzo Gomez, R. Losito, S. Mariotto, M. Mentink, T. Mulder, R. Musenich, D. Novelli, T. Ogitsu, M. Palmer, J. Pavan, H. Piekarz, A. Portone, L. Quettier, E. Rochepault, L. Rossi, T. Salmi, H. Schneider-Muntau, C. Senatore, M. Statera, H. Ten Kate, P. Testoni, G. Vallone, A. Verweij, R. Van Weelderen, M. Wozniak, A. Yamamoto, Y. Yang, Y. Zhai, and A. Zlobin, "Magnets for a Muon Collider—Needs and Plans," *IEEE Trans. Appl. Supercond.*, vol. 34, no. 5, 2024, Art. no. 4005708.

[8] V. Kashikhin, "HTS Accelerator Magnets Conceptual Design for Future Lepton Colliders," *IEEE Trans. Appl. Supercond.*, vol. 34, no. 5, 2024, Art. no. 4605105.

[9] Y. Yang, M. Yoshida, T. Ogitsu, Y. Makida, T. Nakamoto, T. Okamura, K. Sasaki, and M. Sugano, "Influence of neutron irradiation on conduction cooling superconducting magnets," *IOP Conference Series: Materials Science and Engineering*, vol. 101, no. 1, p. 012054, nov 2015. [Online]. Available: https://dx.doi.org/10.1088/1757-899X/101/1/012054

[10] G. A. Kirby, J. Van Nugteren, H. Bajas, V. Benda, A. Ballarino, M. Bajko, L. Bottura, K. Broekens, M. Canale, A. Chiuchiolo *et al.*, "First cold powering test of REBCO roebel wound coil for the EuCARD2 future magnet development project," *IEEE Transactions on Applied Superconductivity*, vol. 27, no. 4, pp. 1–7, 2017.

[11] J. Van Nugteren, G. Kirby, G. De Rijk, L. Rossi, H. H. ten Kate, and M. M. Dhalle, "Study of a 5 T research dipole insert-magnet using an anisotropic ReBCO Roebel cable," *IEEE transactions on applied superconductivity*, vol. 25, no. 3, pp. 1–5, 2014.

[12] M. Dhakarwal, M. Iio, K. Suzuki, M. Yoshida, T. Nakamoto, T. Ogitsu, M. Sugano, K. Tsuchiya, X. Wang, R. Gupta, T. Shen, Y. Yang, and G. Nishijima, "Development and Testing of HTS Coil With Ceramic Coated REBCO Conductor for High Radiation Tolerance," *IEEE Trans. Appl. Supercond.*, vol. 34, no. 5, 2024, Art. no. 4603805.

[13] S. Hahn, K. Kim, K. Kim, X. Hu, T. Painter, I. Dixon, S. Kim, K. R. Bhattarai, S. Noguchi, J. Jaroszynski *et al.*, "45.5-tesla direct-current magnetic field generated with a high-temperature superconducting magnet," *Nature*, vol. 570, no. 7762, pp. 496–499, 2019.

[14] H. Bai, M. D. Bird, L. D. Cooley, I. R. Dixon, K. L. Kim, D. C. Larbalestier, W. S. Marshall, U. P. Trociewitz, H. W. Weijers, D. V. Abraimov, and G. S. Boebinger, "The 40 T Superconducting Magnet Project at the National High Magnetic Field Laboratory," *IEEE Trans. Appl. Supercond.*, vol. 30, no. 4, 2020, Art. no. 4300405.

[15] Y. Yan, Y. Li, and T. Qu, "Screening current induced magnetic field and stress in ultra-high-field magnets using REBCO coated conductors," *Supercond. Sci. Technol.*, vol. 35, no. 1, Dec 2021, Art. no. 014003.

[16] H. Zhang, M. Zhang, and W. Yuan, "An efficient 3D finite element method model based on the T–A formulation for superconducting coated conductors," *Supercond. Sci. Technol.*, vol. 30, no. 2, Dec 2016, Art. no. 024005.

[17] R. Gupta, M. Anerella, J. Cozzolino, P. Joshi, W. Sampson, P. Wanderer, J. Kolonko, D. Larson, R. Scanlan, R. Weggel *et al.*, "Design, construction, and test of HTS/LTS hybrid dipole," *IEEE Trans. Appl. Supercond.*, vol. 28, no. 3, 2018, Art. no. 4002305.

[18] Introduction of FUJIKURA Rare-Earth-based Superconducting Wire. [Online]. Available: https://www.fujikura.co.jp/eng/products/newbusiness/superconductors/01/2052504_12808.html

[19] J. Van Nugteren, "High Temperature Superconductor Accelerator Magnets," 2016, presented 10 Nov 2016. [Online]. Available: https://cds.cern.ch/record/2228249

[20] J. Xia, H. Bai, H. Yong, H. W. Weijers, T. A. Painter, and M. D. Bird, "Stress and strain analysis of a REBCO high field coil based on the distribution of shielding current," *Supercond. Sci. Technol.*, vol. 32, no. 9, Jul 2019, Art. no. 095005.

[21] Y. Yang, K. Mizushima, S. Matsuba, T. Fujimoto, E. Noda, M. Urata, Y. Iwata, and T. Shirai, "Analysis of the magnetization-induced field error in a superconducting bending magnet for a compact, rapid-cycling heavy-ion synchrotron," *IEEE Transactions on Applied Superconductivity*, vol. 33, no. 5, pp. 1–6, 2023.

[22] D. Uglietti, "A review of commercial high temperature superconducting materials for large magnets: from wires and tapes to cables and conductors," *Superconductor Science and Technology*, vol. 32, no. 5, p. 053001, apr 2019. [Online]. Available: https://dx.doi.org/10.1088/1361-6668/ab06a2